25th European Photovoltaic Solar Energy Conference and Exhibition /
5th World Conference on Photovoltaic Energy Conversion, 6-10 September 2010, Valencia, Spain

VERY LOW EMITTER SATURATION CURRENT DENSITIES ON ION IMPLANTED BORON EMITTERS

J. Benick[1], N. Bateman[2], M. Hermle[1]
[1]Fraunhofer Institute for Solar Energy Systems (ISE), Heidenhofstrasse 2, D-79110 Freiburg, Germany
[2]Varian Semiconductor Equipment Associates, 35 Dory Road, Gloucester, MA 01939, USA

Phone +49-761-4588-5493; Fax +49-761-4588-9250; email: jan.benick@ise.fraunhofer.de

ABSTRACT: Ion implantation is the technique of choice for introducing dopant species into semiconductors in CMOS devices. In photovoltaics ion implantation could be an interesting alternative to tube furnace diffusion processes. However, one issue of major importance concerning ion implantation always is the removal of the damage introduced by the implantation process as solar cells always require a defect free, perfectly passivated surface. Thus the surface quality and passivation of boron and phosphorus implanted samples was investigated within this work. It has been found that after an appropriate annealing the introduced damage of both boron and phosphorus implanted surfaces can be completely removed. Very low saturation current densities of <25 fA/cm^2 could be achieved for both boron and phosphorus implanted surfaces after passivation with Al_2O_3 and SiO_2 respectively. On *n*-type back junction solar cells were both the phosphorus FSF as well as the boron emitter have been realized by ion implantation conversion efficiencies up to 19.4% could be achieved.

Keywords: Silicon, Ion Implantation, Passivation

1 INTRODUCTION

The dominant process for the realization of the emitter region of a solar cell is tube furnace diffusion. However, most advanced high-efficiency solar cell structures feature several differently doped areas, e.g. selective emitters and interdigitated patterns (IBC solar cells), leading to new requirements on the respective doping processes. Single side processes are required by almost every advanced structure. Almost as important is an easy structuring of the doped areas as is the case for a selective emitter as well as for the interdigitated structure of the rear side of an IBC solar cell. An independent optimization of the differently doped areas also is of growing interest for future solar cell structures.

Ion implantation is known for a more precise control and reproducibility of impurity dopings and thus has been established as the standard doping process in CMOS fabrication. In photovoltaics ion implantation could be an interesting alternative for tube furnace diffusion processes. Ion implantation inherently is a single side process which can be easily masked by shadow masks or by a simple resist. Other beneficial features of the implantation process are that no doped glass (PSG, BSG) is formed during the doping process and that implantation is a low temperature process that allows independent optimization of differently doped areas. When all implantation processes are finished only a single common high temperature step is needed to activate the implanted dopants. Especially, for the realization of boron doped areas, where the diffusion process is known to be more complicated than for phosphorus, ion implantation might be a promising option.

This paper addresses the question of crystal damage introduced by the implantation process. Fundamentally the question is to what extent the surface damage can be removed by an appropriate annealing process and if an effective passivation of the ion implanted surfaces is possible, as solar cells in general and high-efficiency solar cells in particular require a defect free perfectly passivated surface.

Thus, in this work the passivation of boron and phosphorus implanted surfaces will be investigated and both boron and phosphorus implantation will be applied on *n*-type back junction solar cells.

2 BORON IMPLANTATION

2.1 Experimental

For the evaluation of the ion implantation process with respect to surface damage as well as lateral homogeneity 100 Ω cm *n*-type FZ 4 inch silicon wafers received a boron implantation process on both sides. The implants were performed on a Varian implanter at the Varian factory. As a reference some wafers (10 Ω cm) received a BBr_3 tube furnace diffusion at 890°C instead of the implantation process. After removing the boron glass of the diffused samples and a subsequent surface cleaning by a HNO_3 etch followed by a short HF (1%) dip, all samples received an annealing process in the tube furnace at high temperature. For the surface passivation a dry thermal oxide was grown during the annealing step. On some samples the SiO_2 was removed again in HF and the surface was passivated by PA-ALD Al_2O_3. As the last step the samples received an annealing in forming gas and the injection dependent lifetime was measured by the QSSPC method [1]. From the measured lifetime the emitter saturation current density (J_{0e}) has been calculated by the high injection method [2, 3]. The schematic cross section of the boron doped lifetime samples is shown in Fig. 1.

To measure the lateral uniformity of the sheet resistance of the ion implanted as well as the diffused wafers, the SiO_2 was removed and the sheet resistance was measured via the four point probe technique. The resulting doping profiles were measured with ECV.

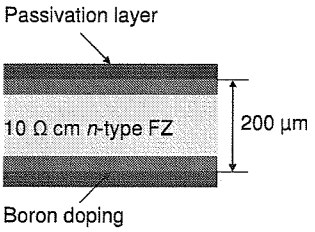

Fig. 1 Schematic cross section of the boron doped lifetime samples.

2.2 Results

The resulting doping profiles of the diffused and the implanted boron emitter are shown in Fig. 2. As can be seen both profiles are quite comparable and feature a low surface doping concentration in the range between 5×10^{18} - 6×10^{18} cm^{-3} and a depth of about 1.5 µm.

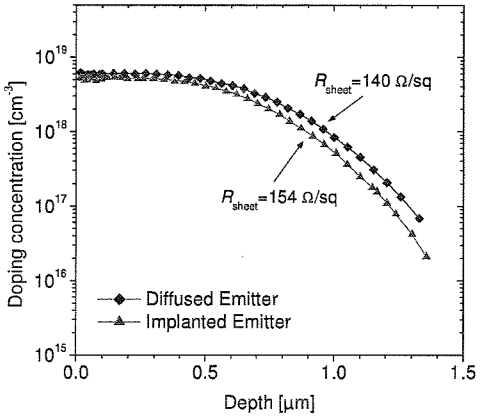

Fig. 2 Doping profiles of the BBr_3 tube diffused as well as the Ion Implanted boron emitter.

Fig. 3 shows the sheet resistance measurements of the boron diffused as well as the boron implanted sample. As can be seen, both processes the BBr_3 tube diffusion as well as the ion implantation provide a uniform doping distribution over the investigated 4'' wafers. However, a higher uniformity can be reached by the ion implantation process (standard deviation ~0.5% for the implanted compared to ~3% for the diffused boron emitter). The sheet resistances of the different emitter samples are ~150 Ω/sq for the ion implanted and ~140 Ω/sq for the diffused boron emitter.

To evaluate the implanted boron emitter with respect to a possibly remaining surface damage due to the implantation process, the emitter saturation current density, J_{0e}, was extracted from the injection dependent lifetime measurements (see Fig. 4). As can be seen the $1/\tau_{eff}$-$1/\tau_{Auger}$ plot over the excess carrier concentration shows a perfect linear slope, allowing for an accurate determination of J_{0e}.

a) Diffused boron emitter b) Implanted boron emitter

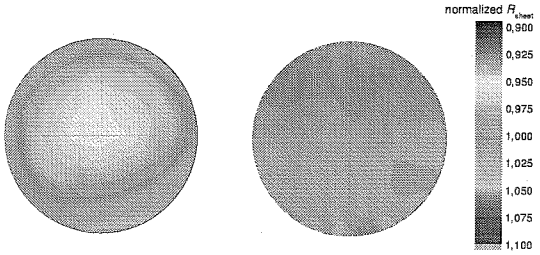

139.8 Ω/sq ±4.3 Ω/sq 153.6 Ω/sq ±0.7 Ω/sq

Fig. 3 Normalized sheet resistance, R_{sheet}, maps of boron doped emitters. Emitter a) is realized by a BBr_3 tube diffusion process and emitter b) by Ion Implantation.

In the case of the SiO_2 passivated rear side the emitter saturation current densities of the diffused and the implanted sample are quite comparable. However, due to the moderate passivation quality of the SiO_2 on highly boron doped surfaces, the overall level of the J_{0e} is still relatively high (156 fA/cm² and 151 fA/cm² respectively) and a remaining damage due to the implantation can not be completely excluded. Thus, to provide a nearly perfect surface passivation, the same boron emitters were passivated by PA-ALD Al_2O_3. Extremely low emitter saturation current densities in the range of 20 fA/cm² could be measured for both, the diffused as well as the ion implanted boron emitter, proving that there is no remaining damage due to the ion implantation process. Based on the also very high effective minority carrier lifetime (see Table I) it can also be stated that the quality of the bulk material is not affected by the implantation process [4].

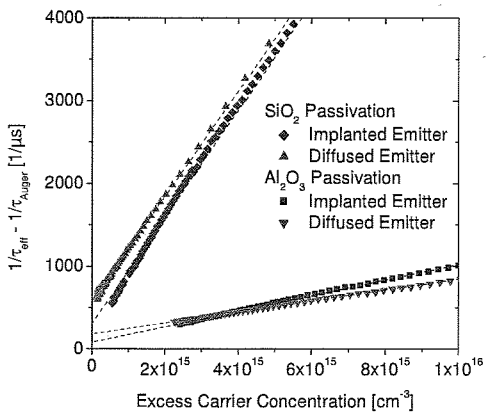

Fig. 2 $1/\tau_{eff}$-$1/\tau_{Auger}$ versus Δn to extract the emitter saturation current density (J_{0e}) of the boron doped samples.

Table I Effective lifetime (τ_{eff}, measured at $\Delta n = 10^{15}$ cm^{-3}), emitter saturation current density (J_{0e}) and implied V_{oc} of the boron doped samples passivated with SiO_2 and Al_2O_3.

	τ_{eff} [ms]	J_{0e} [fA/cm^2]	Imp. V_{oc} [mV]
	SiO_2		
Diffused Emitter	0.80	151	668
Implanted Emitter	0.92	156	667
	Al_2O_3		
Diffused Emitter	4.1	14	719
Implanted Emitter	6.1	20	714

3 PHOSPHORUS IMPLANTATION

2.1 Experimental

For the evaluation of the ion implantation process with respect to surface damage 10 Ω cm *n*-type FZ 4 inch silicon wafers received a phosphorus implantation process at 30 keV on both sides. In the same was as the boron implanted samples the phosphorus implanted samples received an annealing process in the tube furnace at the same temperature as the boron samples. For the surface passivation a thin thermal oxide (10 nm) was grown and covered by a 60 nm thick layer of PECVD SiN_x. As the last step the phosphorus implanted samples received an annealing in forming gas as well and the injection dependent lifetime was measured by the QSSPC method. The resulting doping profile also was measured with ECV. The schematic cross section of the phosphorus implanted lifetime samples is shown in Fig. 5.

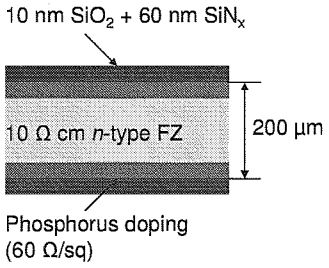

Fig. 3 Boron diffusion profiles of the industrial type as well as the high-efficiency type emitter.

2.2 Results

The resulting profile of the phosphorus implantation is shown in Fig. 6. The profile has a surface concentration of 5×10^{18} cm^{-3} and a depth of ~1.5 µm. The sheet resistance of the final phosphorus implanted profile is about 100 Ω/sq.

As for the boron implanted profiles the saturation current density is extracted from the injection dependent minority carrier lifetime (see Fig. 7). Just like the boron implanted sample the $1/\tau_{eff}$-$1/\tau_{Auger}$ plot for the phosphorus sample shows a perfect linear slope, allowing for an accurate determination of J_{0s}. The resulting J_{0s} of the phosphorus implanted sample with about 24 fA/cm^2 also is very low, again proving that the surface damage introduced by the implantation process can be completely removed by an appropriate annealing process.

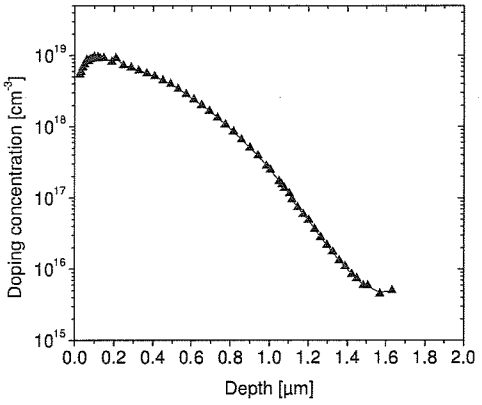

Fig. 4 Doping profile of the phosphorus implanted FSF.

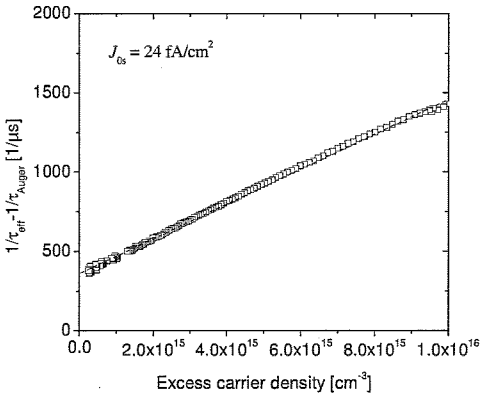

Fig. 5 $1/\tau_{eff}$-$1/\tau_{Auger}$ versus Δn to extract the saturation current density (J_{0s}) of the phosphorus implanted sample.

Table II Effective lifetime (τ_{eff}, measured at $\Delta n = 10^{15}$ cm^{-3}) and saturation current density (J_{0s}) of the phosphorus implanted sample passivated with SiO_2.

	τ_{eff} [ms]	J_{0s} [fA/cm^2]
Phosphorus implant	2.2	24

4 SOLAR CELLS

3.1 Experimental

Small area (4 cm^2) *n*-type back junction solar cells have been processed to investigate the boron implanted emitter as well as the phosphorus implanted front surface field (FSF) at the device level. The back junction solar cells have been fabricated on ⟨100⟩ 1 Ω cm and 10 Ω cm, FZ, *n*-type silicon wafers with a thickness of 200 µm. The processing of these solar cells starts with the formation of the random pyramids textured front. In the next step the phosphorus FSF as well as the boron emitter have been implanted. The implantation conditions applied are identical to those applied for the lifetime samples. After the implantation the cells received an

annealing process in the tube furnace at high temperature. For the surface passivation a dry thermal oxide was grown during the annealing step. At the front side this oxide is removed and a very thin SiO_2 (10 nm) is grown and covered by a SiN_x antireflection coating (60 nm). For some cells the SiO_2 also was removed from the rear side and the rear side then was passivated by an Al_2O_3/SiO_x layer stack. After the surface passivation the contact openings have been photolithographically defined and the Ti/Pd/Ag front contacts have been evaporated and the cells then achieved an annealing in forming gas (425°C). In the next step the rear side contact openings also have been photolithographically opened and the Al rear contact has been evaporated. As a last step the front contacts have been thickened by a plating step and the cells have been separated in a sawing process (margin of 5 mm to the active cell area). The final structure of this ion implanted back junction solar cells is shown in Fig. 8.

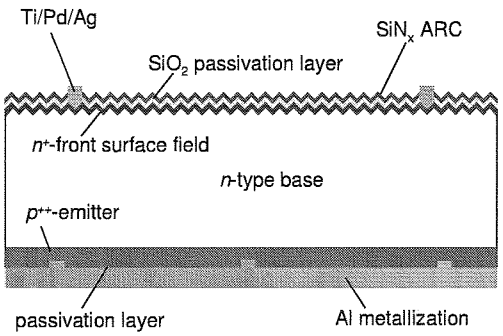

Fig. 6 Schematic cross section of the back junction solar cell structure.

3.2 Results

The one-sun parameters of the *n*-type back junction solar cells featuring the boron implanted emitter as well as the phosphorus implanted FSF are summarized in Table III. Conversion efficiencies of 19.0% for the SiO_2 and 19.4 for the Al_2O_3 passivated cells could be reached. While the short circuit current density J_{sc} is quite high for these cells (40.1 mA/cm^2 and 39.8 mA/cm^2, respectively) the V_{oc} is relatively low. Based on the low J_{0e} achieved for the lifetime samples higher V_{oc} in the range of 660 mV for the SiO_2 and >680 mV for the Al_2O_3 passivated cells would have been expected.

Table III One-sun parameters of the ion implanted back junction solar cells (AM1.5G (Ed.1), 100 mW/cm^2, 25°C, aperture area measurement).

	V_{oc} [mV]	J_{sc} [mA/cm^2]	*FF* [%]	η [%]
	SiO_2 rear side passivation			
1 Ω cm	622.4	38.3	77.6	18.5
10 Ω cm	621.7	40.1	76.2	19.0
	Al_2O_3 rear side passivation			
10 Ω cm	630.7	39.8	77.3	19.4

The quantum efficiency of the SiO_2 as well as the Al_2O_3 passivated cells is shown in Fig. 9. Over a wide wavelength range (300 nm to 1000 nm) the IQE ≥ 95%. Particularly in the short wavelength range this proves that the phosphorus implanted FSF is efficiently passivated by the SiO_2/SiN_x layer stack, especially as back junction cells always are very sensitive to the front side passivation. The overall relatively high level of the IQE further shows that the Si bulk is not damaged by the implantation process or the combination between implantation/annealing [4]. Thus the reason of the low V_{oc} might be attributed to the rear side boron emitter. The reason for the low V_{oc} and the differences between lifetime samples and solar cell results not clear yet and a more detailed microscopic analysis of the cells is under way.

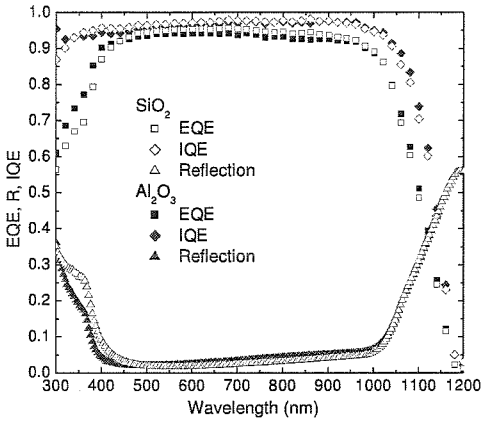

Fig. 7 IQE, EQE and reflection of the ion implanted back junction solar cells where the rear side is passivated by SiO_2 and Al_2O_3 respectively.

5 CONCLUSIONS

In this work the surface passivation of boron and phosphorus implanted surfaces has been investigated. On Al_2O_3 passivated boron implanted samples both very low emitter saturation current densities of 20 fA/cm^2 as well as a high effective minority carrier lifetime above 6 ms could be measured after an appropriate annealing. Also for the SiO_2 passivated phosphorus implanted sample very low saturation current densities in the range of 25 fA/cm^2 and a high effective minority carrier lifetime of 2.2 ms could be measured. This proves that the surface damage introduced by the implantation process can be completely removed by an appropriate annealing.

On *n*-type back junction solar cells with implanted FSF and emitter conversion efficiencies up to 19.4% could be achieved.

6 ACKNOWLEDGEMENTS

The authors would like to thank S. Seitz, I. Druschke, A. Leimenstoll and F. Schätzle for processing and E. Schäffer for measurements.

7 REFERENCES

[1] R.A. Sinton, A. Cuevas and M. Stuckings, Proceedings of the 25th IEEE Photovoltaic Specialists Conference, Washington DC, USA (1996) 457.
[2] D.E. Kane and R.M. Swanson, Proceedings of the 18th IEEE Photovoltaic Specialists Conference, Las Vegas, Nevada, USA (1985) 578.
[3] A. Cuevas and D. Macdonald, Solar Energy 76 (2004) 255.
[4] D. Macdonald, H. Maeckel, S. Doshi, W. Brendle and A. Cuevas, Applied Physics Letters 82 (2003) 2987.